UC Irvine

UC Irvine Previously Published Works

Title

Versatile Bottom-Up Synthesis of Tethered Bilayer Lipid Membranes on Nanoelectronic Biosensor Devices.

Permalink

Journal

Authors

Zhou, Weiwei
Burke, Peter

Publication Date

DOI

Peer reviewed

Versatile Bottom-Up Synthesis of Tethered Bilayer Lipid Membranes on Nanoelectronic Biosensor Devices

Weiwei Zhou and **Peter J. Burke**[*]

Integrated Nanosystems Research Facility, Department of Electrical Engineering and Computer Science, University of California at Irvine, Irvine, California 92697, United States

Abstract

Interfacing nanoelectronic devices with cell membranes can enable multiplexed detection of fundamental biological processes (such as signal transduction, electrophysiology, and import/export control) even down to the single ion channel level, which can lead to a variety of applications in pharmacology and clinical diagnosis. Therefore, it is necessary to understand and control the chemical and electrical interface between the device and the lipid bilayer membrane. Here, we develop a simple bottom-up approach to assemble tethered bilayer lipid membranes (tBLMs) on silicon wafers and glass slides, using a covalent tether attachment chemistry based on silane functionalization, followed by step-by-step stacking of two other functional molecular building blocks (oligo-poly(ethylene glycol) (PEG) and lipid). A standard vesicle fusion process was used to complete the bilayer formation. The monolayer synthetic scheme includes three well-established chemical reactions: self-assembly, epoxy-amine reaction, and EDC/NHS cross-linking reaction. All three reactions are facile and simple and can be easily implemented in many research labs, on the basis of common, commercially available precursors using mild reaction conditions. The oligo-PEG acts as the hydrophilic spacer, a key role in the formation of a homogeneous bilayer membrane. To explore the broad applicability of this approach, we have further demonstrated the formation of tBLMs on three common classes of (nano)electronic biosensor devices: indium-tin oxide-coated glass, silicon nanoribbon devices, and high-density single-walled carbon nanotubes (SWNT) networks on glass. More importantly, we incorporated alemethicin into tBLMs and realized the real-time recording of single ion channel activity with high sensitivity and high temporal resolution using the tBLMs/SWNT network transistor hybrid platform. This approach can provide a covalently bonded lipid coating on the oxide layer of nanoelectronic devices, which will enable a variety of applications in the emerging field of nanoelectronic interfaces to electrophysiology.
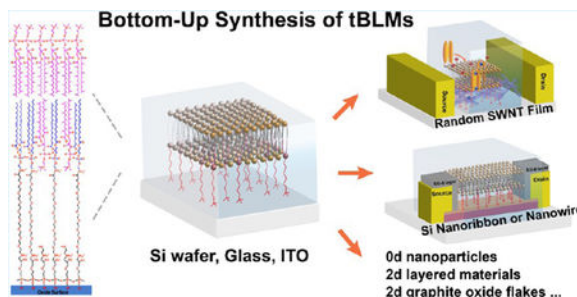
Graphical Abstract

[*]**Corresponding Author**: pburke@uci.edu. Tel: (949) 824-9326. Fax: (949) 824-3732.

Keywords

tethered bilayer lipid membranes; silicon wafer; glass slide; indium-tin oxide; silicon nanoribbon; single-walled carbon nanotube film; biosensor

---

1.   INTRODUCTION

Nanoelectronic probes can be used to interrogate biophysical properties, an emerging theme in the life sciences.[1] Of particular interest is the electrophysiological activity of cell membranes and even organelle membranes. Although model systems such as the black lipid membrane (lipid bilayers suspended over an orifice) allow classical interrogation of electrophysiological function with exquisite precision, it lacks the scalability of modern micro and nanoelectronics. In order to more directly interface state of the art nanoelectronic devices with lipid bilayer electrophysiology, a more intimate and chemically well-defined interface between active electronic devices and lipid bilayers is required.

To date, this has been accomplished using direct physisorption of lipid bilayers onto the nanostructures themselves, including, for example, silicon nanowires,[2] GaP nanowires,[3] carbon nanotubes,[4] and nanoparticles.[5] These studies are based on over a decade of experience of attaching lipid bilayers to solid supports using a variety of noncovalent attachment schemes, including solid-supported lipid bilayers (s-SLBs) and polymer-cushioned/SLBs.[6–12] We have recently developed a polymer-cushioned lipid bilayer/single-walled carbon nanotube (SWNT) transistor platform through three noncovalent polymer functionalization schemes and successfully demonstrated single ion channel sensing using this platform.[13] Additionally, we have previously developed an analogous demonstration using a SLB-graphene platform.[14] In the meantime, other groups have interfaced silicon nanowire electronics with model SLBs and proteins at the ensemble level.[15] At the cellular scale, a variety of approaches are under development to replace the patch clamp pipette technique (nanostraw, nanopipette, nanopillar, etc.) with a nanowire-type approach.[16–20] All of these approaches and goals depend crucially on the interface between the nanostructure and the lipid bilayer membrane. Solid-supported and polymer-cushioned methods inherently lack molecular precision and chemical stability at the interface between the lipid bilayer and the nanostructure. For example, although some advances have been made in lipid bilayer silicon hybrid devices using SLBs,[2,3,15,20] this type of lipid membrane fails to address a serious issue: the spacing between lipid bilayers and solid substrate is not well-controlled, typically between 0.5 and 2 nm due to direct support.[9] This spacing is insufficient for

providing an aqueous layer to completely separate lipid bilayers from the substrates, resulting in strong interactions between membranes and substrates with a high risk of membrane protein[21] Also, the noncovalently attached bilayers have limited lifetimes (minutes to hours). It is desirable to develop a feasible approach to synthesize a more robust and chemically well-defined interface between the nanostructure and the lipid bilayer membrane.

In this work, we develop and demonstrate a covalent tether attachment chemistry based on silane functionalization of the commonly occurring —OH groups that are found on the oxide coating of most nanoelectronic devices, followed by step-by-step stacking of two other functional molecular blocks: oligopoly(ethylene glycol) (PEG) and lipid. As the surface of most nanostructures/nanoelectronic devices includes a dielectric coating between the active electronic channel and the physiologically relevant electrolyte, the oxide material becomes the most common and important target for attaching lipid bilayers on the nanostructures/ nanoelectronic devices. The architecture of the monolayer. we designed from bottom to top, consists of a self-assembled monolayer (SAM) of 3-glycidyloxypropyltrimethoxysilane (GOPS), an oligo-PEG (carboxyl-(ethylene glycol)$_8$-amine compound (CA(PEG)$_8$)) layer providing a hydrophilic reservoir, and a 1,2-dioleoyl-*sn*-glycero-3-phosphoethanolamine (DOPE) lipid layer. This heterofunctional oligo-PEG molecule containing terminal amine and carboxyl groups also serves as a biocrosslinker covalently conjugated with lipids and silane layers on each side. The synthetic route of monolayer functionalization includes three well-established chemical reactions: self-assembly,[22] epoxy-amine reaction,[23] and the EDC/NHS cross-linking reaction.[24] The reactions are facile and simple and can be easily implemented in many research labs on the basis of common, commercially available precursors and mild reaction conditions.

We performed the usual soft-material characterization of the resulting biomembrane, including fluorescence imaging, X-ray photoelectron spectroscopy (XPS), and atomic force microscopy (AFM). The functionalized surface after each reaction step was characterized by AFM and XPS for monitoring the evolution of surface morphology and identifying the chemical compositions of surface groups, respectively. The tethered bilayer lipid membranes (tBLMs) were prepared on monolayerfunctionalized substrates by the vesicle fusion (VF) method. The surface morphology, continuity, and fluidity of the tBLMs were sequentially measured by AFM, fluorescence microscopy, and fluorescence recovery after the photobleaching (FRAP) technique. For nanoelectronics biosensing applications, in contrast to most works on lipid bilayer chemistry, electrochemical impedance spectroscopy (EIS) was employed to monitor the formation of tBLMs and probe the incorporation of the ion channel protein a-hemolysin (a-HL).

To explore the applicability of this approach, we have demonstrated this approach on three common classes of nanoelectronic biosensor candidates: indium-tin oxide (ITO)-coated glass, silicon nanoribbon devices, and high-density single-walled carbon nanotubes (SWNT) networks on glass. Moreover, after incorporating the ion channel peptide alamethicin into the tBLM on the SWNT network transistor, we have detected ion channel currents through alamethicin channels using this tBLM-SWNT transistor hybrid biosensor platform.

Therefore, this tBLM can provide a biocompatible and functional interface for hosting ion channels or other membrane proteins to be integrated with nanoelectronic devices.

This work on nanoelectronics platforms is enabled by the pioneering work done over 10 years ago on the covalent tether chemistry of lipid bilayers on Au using thiol conjugation chemistry, developed by Cornell et al.[25–27] and followed up by other research teams[28–32] and the silane tether chemistry of lipid bilayers on silicon wafer developed by Ingo Köper et al.[33] The advantage of the approach developed on Au by Cornell et al. (and later by follow-on work) as compared with the physisorption approach with polymer cushions is that the covalently linked spacer molecule can allow for control of the water layer thickness between the tBLM and the substrate. By using different oligo spacer lengths, both Cornell (using EIS[25–27]) and others (using neutron scattering[28–32]) showed that, with this general approach, (1) the water layer thickness between the tBLM and the substrate could be controlled, (2) the polymer spacer layers were hydrated, and (3) the insertion of some peptides up to a certain size into the membrane is possible, while maintaining their electrophysiological activity.

Our work has certain advantages over that of Köper et al. Direct synthesis of the silane-oligo-(PEG)$_4$-lipid precursor requires a multistep, complicated organic synthesis process, including critical non-water-based synthesis conditions. Moreover, the unstable silane head group makes the silane precursor unsuitable for long-time storage and shipping; thus, it is not commercially available. In addition, silane-polymer-tethered lipid bilayers on SiO_2 substrates have been reported by Tamm et al.[34] and Andruzzi et al.[35] using two different length polymer PEGs, respectively, containing 77 unit ethylene glycol and 45 unit ethylene glycol. However, neither electrochemical measurements nor electrophysiological recordings have been reported in their studies.

Thus, although the thiol chemistry of gold is well established, it is not amenable to integration with nanoelectronic devices made of semiconducting materials, such as nanowires, nanotubes, and 2d materials. Therefore, even though our work is not as extensive as that of prior researchers on Au (e.g., we have not performed detailed neutron reflection to measure the detailed water layer between the bilayer and the substrate, and we have not measured many different tether lengths or chemistries), it is much more powerful and significant in terms of the applications to nanoelectronics rather than to gold. In the past, each time a new tether molecule was developed, it turned into an entirely new major paper/study, for example, "WC14" (an EO 6-mer[28]), "FC16" (an EO 9-mer[29]), and "HC18" (an EO 6-mer with unsaturated anchor molecules[31]). Rather than being an evolutionary study of the effect of different spacer chemistries, our work uses well known and well-studied spacer chemistry themes (in our case an 8-mer of EO as proof of concept), and provides a dramatically simplified recipe that can be performed by labs with minimal expertise in organic chemistry synthesis, and applies it to open up an entirely new domain of applications of this scheme by (1) demonstrating integration with several example nanoelectronic platforms and (2) demonstrating the ability to sense single ion channel events electrically. This general strategy should find a wide range of applications in the emerging field of nanoelectronic interfaces to electrophysiology.

2. EXPERIMENTAL SECTION

2.1. Reagents and Materials.

The lipids including 1,2-diheptadecanoyl-*sn*-glycero-3-phosphocholine (DPhPC) and DOPE were purchased from Avanti Polar Lipids. The dye lipid Lissamine Rhodamine B 1,2-dihexadecanoyl-*sn*-glycero-3-phosphoethanolamine, triethylammonium salt (LR-DHPE) was purchased from Life Technologies. 1-Ethyl-3-[3-dimethylaminopropyl]carbodiimide hydrochloride (EDC), N-hydroxysuccinimide (NHS), and carboxy-(ethylene glycol)$_8$-ethylamine (CA(PEG)$_8$) were purchased from Thermo Fisher Scientific Inc. Alamethicin, α-hemolysin, GOPS (99%), ITO-coated glass slides with the surface resistivity of 30–60 Ω/sq, and all other chemicals, including solvents and buffers, were purchased from Sigma Aldrich. GOPS was purchased every 6 months and was stored in a vacuum desiccator. Solvents and buFFers were used as received without further purification. DI water was processed by a Sartorious Stedim Arium water purification system to give 18.2 MΩ cm resistivity. Highly doped silicon wafers (boron doped 0.005–0.01 Ω cm) purchased from Rogue Valley Microdevices were used as semiconductor chips and electrodes. The high-density SWNT network was deposited on glass slides of semiconducting nanotube ink purchased from Nanointegris Inc. (IsoNanotubes-S 99%) by the vacuum filtration method.[36] Silicon nanoribbon devices were fabricated using top-down lithographic techniques on 4 in. ultrathin-silicon-on-insulator wafers (Soitec).[37]

2.2. Self-Assembly of GOPS.

The native oxide layer on silicon wafers was stripped away by a buffered oxide etch solution.[38] The freshly etched silicon wafers and cover slides used for later imaging were thoroughly cleaned by hot piranha solution (a mixture of concentrated sulfuric acid and 30% hydrogen peroxide in the ratio of 7:3) for 1 h to generate sufficient —OH groups on the surface before the self-assembly process. Then, the substrates were washed by copious amounts of DI water and dried under a N$_2$ stream and immediately immersed into a GOPS ethanol solution (9 mM) for another 1 h to form a GOPS SAM on substrates with epoxy functional groups, followed by thoroughly rinsing with acetone, methanol, and isopropanol to remove excessive GOPS silane on the surface. After surface modification, all substrates were stored in a desiccator to prevent air pollution for later use. The ITO chips were immersed in a solution of H$_2$O$_2$/NH$_4$OH/H$_2$O (1:1:5, v/v) for 30 min at 80 °C to obtain a uniformly distributed OH group on the ITO surface. The silicon nanoribbon device was cleaned by oxygen plasma at 50 W for 30 s; more hydroxyl groups were generated on the silicon nanoribbon surface by this treatment. For the substrates with SWNT networks, all procedures are the same except using a 1 h hot water bath (60 °C) instead of the piranha bath to increase the surface —OH group density.

2.3. Coupling CA(PEG)$_8$ to GOPS Terminated Surface.

CA(PEG)$_8$ powder was dissolved in a 1× PBS buffer solution (pH 7.4) with 2 mM concentration. The substrates with GOPS monolayers were incubated in the CA(PEG)$_8$ solution at room temperature for 3 h. CA(PEG)$_8$ spacers were coupled onto substrates through the reaction of their primary amine groups with active epoxy groups on the silane monolayer. Then, the substrates were transferred into a 50 mM ethanolamine DI water

solution (pH 9.0) for 30 min to quench unreacted sites, and subsequently washed with PBS buffer, and kept wet for the next step.

2.4. Covalent Conjugation of DOPE to CA(PEG)$_8$-GOPS.

DOPE lipid molecules were covalently tethered on silicon wafer/glass slide surfaces by a two-step EDC/NHS process.[39,40] First, the carboxylic groups at the other end of the spacer CA(PEG)$_8$ functionalized on the substrates were activated for 2 h in MES-buffered saline solution (pH 4.7) with 75 mM EDC and 25 mM NHS.[40] In the meantime, a chloroform solution with DOPE lipids was evaporated under a nitrogen stream for 2 h. The dried lipids were dissolved in an ethanol solution with 1 mM EDC and 2 mM NHS[39] to result in a lipid concentration of ~0.3 mM. Then, the substrates were rinsed with fresh MES buffer, 1× PBS buffer, DI water, and ethanol successively, followed by an immediate immersion in freshly prepared lipid ethanol solution overnight. The next day, the substrates were rinsed with the following solvents (in order): chloroform, acetone, methanol, and isopropanol, and stored in ethanol solution in a glass Petri dish with a glass lid at 4 °C. The substrates must be kept wet during the whole process.

2.5. Preparation of tBLM by the Vesicle Fusion Method.

A chloroform solution containing 4.25 mg DPhPC lipid was evaporated under a nitrogen stream for 2 h, forming a uniform lipid film on the bottom of a glass vessel, and further dried in a desiccator under vacuum overnight. The dried lipid films were rehydrated in 5 mL of 1× PBS buffer to have a lipid concentration of ~1 mM, and sonicated for an hour to make small unilamellar vesicles. Finally, the suspension was extruded at least 20 times through a mini-extruder with a 0.1 μm pore size membrane (Avanti Polar Lipids), until the final solution appeared clean. The lipid vesicle solution was dropped into a homemade wet chamber with substrates, giving an active electrode area of ~0.12 cm^2, and incubated for 2 h at 60 °C, followed by cooling down to room temperature. The unbounded lipids were removed through rinsing with copious 1× PBS buffer. The chip was stored at 4 °C overnight for further characterization.

2.6. AFM and XPS Characterizations.

AFM images were recorded using Agilent Technologies 5500 AFM and operated in ac contact mode (tapping-mode). XPS spectra of the monolayers on functionalized silicon wafers were recorded on a Kratos axis supra system (Kratos Analytical, Manchester, U.K.) using Al Kα as an X-ray source. The resolution was 160 eV in the wide and 20 eV in the region scans of the C$_{1s}$ and N$_{1s}$ peak. All XPS spectra were analyzed with the CasaXPS software. All wafers were thoroughly washed with acetone, methanol, and isopropanol, to ensure the removal of all unbound molecules, and stored in a vacuum desiccator overnight, before being loaded into the XPS chamber.

2.7. Fluorescence Imaging and FRAP.

To obtain fluorescence images, DPhPCs were mixed with 1 mM fluorescent dyes (LR-DHPE) at the molar ratio of 1000:1. FRAP experiments were performed on tBLM on a glass cover slide for studying lipid fluidity using a Zeiss LSM 780 confocal laser microscope with

an excitation laser at 561 nm. The 561 nm laser was set at 100% intensity to bleach a spot in the lipid membrane. The fluorescence recovery was recorded with a 20× objective lens with 20 s intervals between images at a reduced laser power (<4 mW). The diffusion coefficients of tBLMs were calculated by measuring percentage recovery of fluorescent intensity of the bleached spot in time lapse. Another upright fluorescence microscope (Leica DM400B) was used to characterize the tBLM on the silicon nanoribbon surface with a 63× water immersion objective lens at a reduced laser power (5%).

2.8. EIS Characterizations.

EIS was used to investigate the electrochemical properties of tBLMs on highly p-doped silicon wafers using a Gamry model 600 potentiostat. The measurements were performed using a standard three-electrode system. The working, counter, and reference electrodes, respectively, are the silicon wafer, a platinum wire, and an Ag/AgCl wire. In all measurements, the potentials were applied versus the Ag/AgCl electrode. A homemade PDMS wet chamber provides an active electrode area of ~0.12 cm^2. The spectra were recorded for frequencies from 0.1 or 0.01 Hz to 100 kHz at 0 V bias potential with an AC modulation amplitude of 10 mV. The raw data were analyzed by Gamry echem analyst software and using the equivalent circuits consisting of a series resistor and one or two RC meshes. To investigate the insertion of ion channel proteins, the tBLMs were further monitored by EIS, after 1 h of addition of 4 μL of α-HL (0.25 mg/mL ethanolic stock) into the cis chamber (final concentration: 76 nM).

2.9. Fabrication of SWNT Network Transistor.

A microfluidic channel is integrated with SWNT transistors for the delivery of DPhPC vesicles and electrolyte buffers. Source and drain electrodes are patterned by a standard photolithography and lift-off process. The microfluidic channel with a width of 25 μm was placed between source–drain electrode pairs having a channel length of 50 μm and width of 30 μm to isolate the buffer solution from metal electrodes. A Ag/AgCl wire immersed in the electrolyte solution at the channel entrance is used as the reference electrode for applying a voltage to gate SWNTs. The detailed fabrication process of the SWNT transistor biosensor platform was described in our previous study.[13]

2.10. Electrical Measurement and Data Acquisition of Ion Channel Recording.

The voltage-gated ion channel alamethicin was incorporated into preformed tBLM by adding its ethanolic stock solution into a PDMS entrance chamber, resulting in a final concentration of ~5 μM. KCl (0.5 M) in 1× PBS solution was used for recording. Ion channel recordings were performed at an applied potential of +100 mV using a patch-clamp amplifier system, as previously described.[13] A syringe pump was connected to the microfluidic channel to control the flow rate and exchange fluids. Data were low pass filtered at 5 kHz using the four-pole Bessel filter built into the Axopatch 200B and sampled at 10 kHz. Data collection was performed by electrophysiology software (pClamp10) and plotted using Igor Pro.

3. RESULTS AND DISCUSSION

3.1. Bottom-Up Synthesis and Characterizations of Lipid Monolayer on SiO$_2$ Surfaces.

As shown in Scheme 1, three well-established chemical reactions have been performed for bottom-up synthesis of monolayers on the SiO$_2$ surface: (i) self-assembly of silane;[22] (ii) ring addition reaction of the epoxy group with the primary amine for linking the oligo-PEG spacer onto silane;[23] (iii) EDC/NHS two-step reaction for bioconjugation of lipid molecules onto oligo-PEG.[24] (Note that the (EO)x region is disordered and flexible (like a cooked noodle), and the scheme only shows it extended for clarity.) GOPS as an epoxy group-terminated silane molecule has been extensively used for the covalent immobilization of the molecules containing amino groups, especially biomolecules, on SiO$_2$ substrates due to its simple self-assembly process.[23,41–43] Although, it cannot generate highly ordered structures on silicon surface as long-chain alkylsilanes do,[44] the SAM of GOPS can still provide a relatively flat surface for subsequently growing or patterning nanostructures on silicon wafers[43] or glass slides.[45] Although aggregation of the GOPS in solution before attachment to the silicon surface is possible, it is a very minor effect, as the AFM images (see Supporting Information) show a relatively uniform surface (surface roughness of ~1 nm). Kuno et al.[41] also reported the rootmean-square roughness of GOPS SAM on silicon to be 0.303 nm.

The SAM of GOPS on glass or SiO$_2$/Si wafers is covalently linked with amine-terminated oligo-PEG (CA(PEG)$_8$) molecules by simply immersing the wafer in 1× PBS buffer solution of CA(PEG)$_8$. To prevent the direct binding of DOPE lipid molecules to unreacted epoxy groups in the following step, ethanolamine was applied to quench unreacted sites on the surface. The carboxyl group at the other end of CA(PEG)$_8$ was activated by EDC/NHS to form a stable intermediate NHS ester, and further reacted with the primary amine groups at the hydrophilic head of DOPE lipids to form amide bonds. The EDC/NHS chemistry is one of the most important approaches in bioconjugation and surface immobilization of biomolecules including small amines, DNA, and proteins on carboxyl-group modified surfaces.[24] We choose CA(PEG)$_8$ as the hydrophilic spacer instead of CA(PEG)$_4$ or CA(PEG)$_{12}$ (also commercially available) due to its suitable arm length (~3.4 nm) in this study. The SWNTs that we used in this work have a diameter range of 1–2 nm, whereas CA(PEG)$_4$ only has an arm length of 1.8 nm. The hydrophilic spacer should have enough length to provide a sufficient hydrophilic reservoir for hosting transmembrane proteins and support ion transport, and lift the proximal lipid leaflet up by an adequate distance from the SWNT network-covered SiO$_2$ substrates, allowing those bilayers to form above the SWNT networks. In the meantime, CA(PEG)$_{12}$ is not chosen because an increased tether length usually yields a looser packing order, which can increase the risk of poor electrical sealing.[46] Moreover, recent research has indicated that the sensitivity of SWNT biosensors can be significantly reduced with the increase of the sensing distance in buffered solutions, due to Debye screening.[47]

We observed that a uniform thin water film formed on the silicon wafer or glass slide surface after 3 h of incubation in CA(PEG)$_8$ solution at room temperature, indicating that the sample surface became more hydrophilic, due to the linkage of the hydrophilic spacer. After the

overnight incubation in lipid ethanol solution at 4 °C, we noticed an obvious dewetting behavior of the sample surface, when a DI water rinsing step was performed, indicating that the surface turned more hydrophobic due to the hydrophobic tails of DOPE lipids that were tethered on the surface. The morphologies of the wet and dried monolayers are dramatically different as shown later in AFM characterization. Therefore, no contact angle measurement was performed because a drying process is required to measure the contact angle, and the measurement would not be representative of the in-solution hydrophobicity. The surface property of the monolayer-functionalized wafer for subsequent bilayer formation is determined by the wet monolayer structure, not the dried monolayer structure.

To verify the chemical compositions of the surface groups, XPS was used to analyze the functionalized silicon wafers after each reaction step, due to its high surface-sensitivity. High-resolution C_{1s} XPS spectra of the surfaces of silicon wafers in different reaction steps are shown in Figure 1a–c. Three carbon components were determined in all three spectra after the deconvolution of the curves: C—C bond at 285.2–285.4 eV, C—O ether bond at 287–287.1 eV and C=O ester bonds or amide bonds at 288.7–289 eV.[35,48] The C_{1s} XPS spectrum of the GOPS-functionalized silicon wafer is shown in Figure 1a, in which the C—O peak at 287 eV corresponds to the epoxide rings and ether moieties of GOPS. The presence of the O—C=O peak at 288.7 eV is probably due to contamination (as it occurs in all samples independent of the functionalization step), which is consistent with other studies. [48] The peak area ratio of C—C to C—O can be quantitatively calculated using CasaXPS, which is 1.5 for the GOPS-functionalized silicon wafer (Figure 1a), and decreases to 1.1 (Figure 1b) because more ether bonds are added into the monolayer structure after the linkage of $CA(PEG)_8$ molecules to GOPS via the reaction of the epoxy group with the primary amine, while it increases to 1.3 (Figure 1c) due to the further conjugation of the DOPE lipid onto the GOPS-CA(PEG)$_8$-functionalized surface after the EDC/NHS two-step reaction. It should be noted that the percentages of C=O bonds, shown in Figure 1b,c, are much higher than that shown in Figure 1a, indicating more COOH or CO—NH bonds were formed in steps (ii) and (iii). In addition, we observed a small nitrogen peak at ~400 eV in the wide scan spectrum of the GOPS-CA(PEG)$_8$-DOPE-functionalized surface (Figure 1d) and further confirmed the presence of the N 1s peak by performing a region scan (Figure 1e).[49] This is important evidence of amide bond formation after the EDC/NHS two-step reaction. Therefore, the XPS results are in good agreement with the chemical structure after each reaction, as shown in Scheme 1.

The morphology evolution of the silicon wafer after each surface functionalization step was monitored by AFM using the ac contact mode (tapping mode) in air and is shown in Figure S1. After each functionalization step, one wafer sample was randomly taken out from the same reaction container, successively rinsed with fresh solvents and DI water, and blown dry under a N_2 stream for AFM characterization. Compared with the bare silicon wafer with an extremely flat surface, the GOPS SAM (Figure S1b) has a noticeable increase of surface roughness, but the morphology can be considered to be uniform and homogenous. The nanoparticles observed on the surface have a height of 1.0 nm. The clusters and largearea domains in Figure S1c with roughnesses of 1.6 nm arise from the dried flexible PEG arms. Furthermore, more clusters were observed on the surface modified with GOPS-CA(PEG)$_8$-DOPE (Figure S1d). A pronounced contrast of particles with uniform sizes and high density

has been observed in a high-magnification phase image (Figure S1f), even though the topographical images do not show significant roughness change (Figure S1d,e). We attribute this to the fact that phase imaging can distinguish materials with different surface properties, due to their different interactions with AFM tips. In contrast to a hydrophilic surface, the hydrophobic tails of tethered DOPE lipids can self-assemble to small particles and therefore become more obvious in the phase image (Figure S1f) than in the topological image (Figure S1e).

The GOPS-CA(PEG)$_8$-DOPE monolayer, without drying, during the synthesis process was characterized by liquid-AFM in 1× PBS solution using tapping mode and AFM probes with low spring constants (~0.3 N/m). Both topological (Figure 2a) and phase (Figure 2b) images clearly illustrate that submicron-sized domains have formed on the silicon wafer after three chemical reactions. The height of the monolayer domains is 5–6 nm, according to the z-scale measurement shown in the height profile chart (Figure 2a), which is a reasonable value, on the basis of the total molecular length of CA(PEG)$_8$ and DOPE lipid.

The phenomenology of domain formation (so-called "clusters") on gold was studied in ref 32, although the mechanism of cluster formation in that case was related to the drying process. Our work is slightly different, in that we observed the domains, even without a drying step. The schematic in Figure 2c shows the molecular interpretation of the domain structure, prior to assembly of the top layer, which is consistent with the AFM images and ref 32. It should be noted that the hydrophobic tails in the monolayer are flexible and bundled together to minimize contact with aqueous solution. Figure 2c is a simplified cartoon for illustration purposes.

3.2. Formation and Characterization of tBLM.

After successful synthesis of the bottom monolayer, a VF process was carried out to form a bilayer lipid membrane on the monolayer surface through incubation with DPhPC vesicles at 60 °C for 2 h. The unbounded lipids were removed from the wafer surface by rinsing with copious 1× PBS buffer after slowly cooling down to room temperature. The wafer was stored at 4 °C for further overnight incubation. Liquid-AFM characterization was performed on day 2. The topological image (Figure 2d) shows a smooth surface with a roughness of <1 nm, and the phase image (Figure 2e) illustrates that tBLM has a more uniform surface property than the monolayer (Figure 2b). (More AFM images of the monolayer and tBLMs are shown in Figure S2.) Thus, although the domains provide inhomogeneity, which, ideally, should be minimized in future work, in this work, they did not prevent the formation of complete surface coverage of the lipid bilayers, as shown in Figure 2d, after complete assembly. The schematic (Figure 2f) shows the interpretation of the final tBLM structure. The AFM image clearly shows a uniform, smooth tBLM surface with less than 1 nm roughness after final assembly, confirming that the final tBLM provides complete surface coverage.

To conclude, both XPS and AFM results have confirmed the formation of the GOPS-CA(PEG)$_8$-DOPE monolayer on SiO$_2$ substrates via our bottom-up approach presented in Scheme 1. The surface coverage and height of monolayers could be further tailored, according to research purposes, by massively screening different arm-length spacers and

optimizing ratios of mixed long/short spacers, for example, CA(PEG)$_8$/methyl-(ethylene glycol)$_4$-amine (MA(PEG)$_4$). As a "proof-of-concept" demonstration, we only focus on studying the CA(PEG)$_8$ spacer in this article.

To perform fluorescence characterization, DPhPCs were mixed with 1 mM fluorescent dyes (LR-DHPE) at a molar ratio of 1000:1. Fluorescence imaging (Figure 3a) shows that a continuous and uniform film formed on the entire functionalized surface (~0.12 cm^2). The membrane fluidity plays an important role in planar lipid bilayer membranes because it can affect the diffusion or conformational changes of ion channel proteins and other biomolecules within the membrane. Therefore, a FRAP analysis was performed to evaluate the lateral diffusion of tBLM on a glass cover slide. Figure 3c shows the fluorescence images of a sample spot, with a diameter of about 64 μm, recorded before (left), immediately after (middle), and 670 s (right) after photobleaching. According to the plot shown in Figure 3d, the diffusion coefficient, D, for LR-DHPE in the tBLM can be determined by the equation: $D = 0.224r^2/t_{1/2}$, in which r is the radius of the photobleached area, and $t_{1/2}$ is the time required to achieve 50% fluorescence intensity recovery.[50] The calculated D value is ~1.9 μm^2 s^{-1} (an average of three experiments), which is comparable to the FRAP results of the PEG polymer-cushioned[51] or tethered polymer bilayer[34,35] on glass slides (0.8–2.5 μm^2 s^{-1}) in earlier studies. No FRAP data have been reported prior to this work for tBLMs, when oligo-PEG was used as the hydrophilic tether. In addition, we observed only 70% fluorescence intensity recovery after complete recovery compared to the intensity before bleaching, indicating that the tethered membrane has an immobile fraction of ~30%. This effect has been discussed with respect to polymer-tethered or cushion lipid bilayers, and the main reason is the presence of tethered lipids in the proximal leaflet, which behave as immobile obstacles on planar substrates.[34] According to previous studies, immobile fractions have been observed from 0 to 80%, depending on polymer concentrations, and thus the immobile fraction of ~30% in this work corresponds to a relatively low tether density.[34] The same VF process has been performed on the monolayer only consisting of GOPS and DOPE, as DOPE has a primary amine head group, which can directly react with the epoxy group. However, the results of fluorescence imaging of the tBLM without the oligo-PEG spacer show more heterogeneous structures (Figure 3b), which indicates that the oligo-PEG hydrophilic spacer plays a crucial role in forming a uniform tBLM. Another similar experiment has been performed by Casford et al. to covalently tether dipalmitoylphosphatidylethanolamine lipids onto an SAM of mercapto-undecanoic acid (MUA)-modified gold substrate.[52] However, the sum frequency generation vibrational spectra in their paper showed incomplete bilayer or multilayer membrane formation, when the distal leaflet was added by the VF method, indicating that MUA is not a suitable spacer for tBLM due to its long hydrocarbon molecular chain.

We next demonstrated this approach on silicon nanowires (or nanoribbons) for translating this advance to nano/micro systems. The nanowire device is a silicon nanoribbon device fabricated by top-down lithographic techniques.[37] Figure 3f shows a bright field optical image of a 2 μm wide and 20 μm long nanoribbon. A small window in the SU8 protective layer is used to expose the surface of the nanoribbon solution. A 15–20 nm top-oxide layer was grown on the silicon surface by a prior thermal O$_2$ oxidation. Prior to the functionalization process, a gentle oxygen plasma treatment was used to clean the

nanoribbon surface and generate —OH groups. After the monolayer functionalization and VF process, the nanoribbon surface within the small window shows obvious and uniform fluorescence (Figure 3e), which indicates the formation of the tBLM on the silicon nanoribbon.

3.3. Investigation of the Electrical Properties of Monolayer and tBLM on Silicon Wafer by EIS.

We next characterized the electrical properties of the tBLM using EIS. A highly boron-doped (p-type) silicon wafer served as the functionalization substrate and also the working electrode (Figure 4a).[33,53] The EIS data of the bare silicon wafer (Figure S3a) and GOPS-CA(PEG)$_8$-DOPE monolayer-functionalized silicon wafer (black triangle in Figure 4b) were analyzed using an equivalent circuit consisting of a series resistor and an RC mesh Figure 4a (inset). The raw data was analyzed and fitted by Gamry echem analyst software. The capacitance, C_{SiO_2} includes the contributions from the capacitance of the native SiO_2 layer with/without monolayer, the space charge layer capacitance, and the double layer capacitance. The resistance, R_{SiO_2}, represents the charge transfer resistance at the electrolyte/substrate interface. After functionalization, C_{SiO_2} calculated from the EIS data slightly decreased from 2.3 to 2.2 μF cm^{-2}, due to the additional thickness of the tethered monolayer on silicon,[33] while R_{SiO_2} significantly increased from 1.2 to 10.0 MΩ cm^2 (Table 1), which can be ascribed to the influence of the GOPSCA(PEG)$_8$-DOPE monolayer tethered on silicon that prevents the silicon electrode from coming into direct contact with the electrolyte solution and introduces a more complicated solid/monolayer-liquid interface. After 2 h incubation of the monolayer-functionalized silicon wafer with DPhPC vesicles, a shoulder impedance peak and the corresponding phase peak promptly rose in the middle-frequency region of the Bode plot, indicating that another RC mesh had started to form. Hence R_{mem} and C_{mem} are added into the equivalent circuit (Figure 4a inset) to describe the resistance and capacitance of the tethered bilayer membrane. After further overnight incubation, R_{mem} was steady at 42.7 kΩ cm^2 and C_{mem} was 0.9 μF cm^{-2}. The capacitance of tBLMs dominates in the middle-frequency region of the Bode plot, whereas the capacitance of the silicon substrate dominates in the low-frequency region. The two regions are separated by the shoulder (red circle in Figure 4b), whose position is determined by the resistance of tBLM. The fit R, C values are shown in Table 1.

To confirm that electrically active membrane proteins can be inserted into the bilayer successfully, we next measured EIS after incubation with (and incorporation of) a-HL. The a-HL is a very conductive pore, and the incorporation of many of these is expected to significantly change the membrane resistance, without changing its capacitance. As expected, after 1 h incubation with a-HL at room temperature, the resistance of the tBLM rapidly decreased to 8.9 kΩ cm^2 and the capacitance stayed the same at 0.9 μF cm^{-2} (blue circle in Figure 4b). We have performed control experiments and found that without any ion channel incorporation, the tethered bilayer membrane is stable for a week, when stored at 4 °C. As shown in Figure S3b, the resistance of tBLM fell from 31 to 14 kΩ cm^2, after 1 week, suggesting all measurements should be performed within 1 week. The capacitance of

tBLM is higher than that of a typical black (i.e., suspended) lipid membrane, 0.7 μF cm^{-2}, and in accord with other studies of thiol-based tBLM on gold, consisting of a single anchor and an eight ethylene glycol unit spacer.[46] The R_{mem} value is slightly higher than that of the tBLMs on gold with a similar structure[46] but lower than the reported values of tBLMs on silicon using a synthetic silane precursor with a shorter spacer.[33] This result indicates that the resistance of tBLM could be improved by screening different arm-length spacers and optimizing the ratio of mixed long/short spacers. The value of R_{mem} is in the typical range of transmembrane resistances, 10^4–10^7 kΩ cm^2.[54]

3.4. Formation of tBLMs on ITO Glass.

In addition to SiO$_2$, ITO is also another attractive substrate for silane functionalization, due to its —OH abundant surface, and has been widely demonstrated to covalently immobilize many biomolecules on its surface using silane anchors for the application of impedance biosensors.[55] Therefore, the same functionalization strategy was carried out on ITO. The functionalization process on ITO is the same except that we used a hot solution of H$_2$O$_2$/NH$_4$OH/H$_2$O (1:1:5, v/v) to treat the ITO surface to obtain a uniformly distributed OH group instead of the hot piranha solution. After the VF process, a uniform tBLM formed on the functionalized ITO surface, according to the fluorescence characterization (Figure S4a).

3.5. Investigation of the Formation of SLBs and tBLMs on SWNT Network Transistors.

Interfacing cell membranes with nanoelectronic devices is an emerging theme for in vitro or in vivo study of cell activities; thus, it is important to provide a biocompatible and stable interfacing surface. For example, the SLB/SWNT hybrid structure has shown promising applications in the electrical sensing of membrane-based biological processes.[4,56] Recently, we have demonstrated that SWNT transistors can be used to detect individual ion channel activity using polymer-cushioned SLBs.[13] In contrast to noncovalently attached SLBs, the tBLM can provide a chemically stable interfacing surface with a delicately controlled and well-characterized structure, which is more desirable for reducing the experimental uncertainty and complexity of electrical sensing, especially electrophysiological recording. Therefore, we decided to investigate the formation of tBLMs on SWNT nanostructures. A random SWNT film (Figure 5a) with a density of ~10 SWNT/μm^2 was deposited on a glass slide by the vacuum filtration method from semiconducting nanotube ink purchased from Nanointegris Inc. (IsoNanotubes-S 99%).[36] The SWNTs in the purified inks have a mean diameter of ~1.4 nm and formed a monolayer in most areas (Figure 5a). In contrast to the flat, hydrophilic surface of glass or SiO$_2$/Si wafers, SWNTs have a highly curved structure, rough supporting surface, and hydrophobic surface properties. As a result, lipid bilayers do not form uniform SLBs on a dense SWNT network film. Figure 5b shows that the surface morphology of lipid bilayers duplicated the fiber structures of the underlying SWNT film after the VF process, indicating that lipid tails tend to be self-assembled on carbon nanotube walls via hydrophobic interactions rather than spread as a film. Other inhomogeneous features, such as bright spots, were observed on SWNT supports. In contrast, the fluorescence of tBLM formed on monolayer-functionalized surfaces, using our new approach developed above, is more homogenous (Figure 5c). All monolayer functionalization processes are the same as those on bare glass slides, except that a 1 h hot water bath (60 °C) was used to increase the surface —OH group density, instead of the

piranha bath. Therefore, it can be concluded that the hydrophilic spacer CA(PEG)$_8$ can effectively lift up the lipid bilayer away from the rough SWNT surface and thus prevent the absorption of lipid molecules on carbon nanotube sidewalls. In the meantime, SWNTs, in this approach, can not only serve as an electrically active readout but also as a lateral spacer to generate sparse tethers, which can be beneficial to membrane protein incorporation.

3.6. Study of Single Ion Channel Activity Using a tBLM-SWNT Transistor Platform.

Using this tBLM functionalization approach, we were able to realize the detection of the single ion channel activity on SWNT transistors. As demonstrated in Figure 5d, a microfluidic channel is integrated with SWNT transistors for the delivery of DPhPC vesicles and electrolyte buffers. Source and drain electrodes (inset in Figure 5e) were patterned by a standard photolithography and lift-off process. A microfluidic channel (width = 25 μm) was placed between source−drain electrode pairs, having a channel length of 50 μm and width of 30 μm, to isolate the buffer solution from the metal electrodes. A Ag/AgCl wire, immersed in the electrolyte solution at the channel entrance, is used as the reference electrode for applying a voltage to gate SWNTs. The detailed fabrication process of the SWNT transistor biosensor platform was described in our previous study.[13] The transfer characteristics of a representative electrolyte-gated SWNT transistor presented in Figure 5e show typical p-type FET behavior. As discussed in our previous studies of electrolyte-gated SWNT/graphene FETs,[13,14] there always exists a small faradic current (gate current) from SWNTs/graphene to the electrolyte solution in the range of the applied gate voltage, which, here, is ~1 nA, at an applied gate voltage of V_{gs} = 100 mV (red line in Figure 5f). After the tBLM formed on the transistor surface (Figure 5f), we found that the gate leakage current of the electrolyte-gated SWNT transistor was significantly reduced to ~10 pA at V_{gs} = 100 mV (blue line in Figure 5f). In other words, a 10 GΩ seal was achieved over a 750 μm^2 (25 μm PDMS channel width $\times$ 30 μm electrode width) area and accordingly, the corresponding specific resistance is 7.5 MΩ cm^2. This indicates that a high-quality tBLM has been formed on the surface of the SWNT transistor and behaves as an electrically insulating layer, which can allow high-quality recording of single ion channels by the patch-clamp technique.

Next, the voltage-gated ion channel, alamethicin, was incorporated into the preformed tBLM, by adding its ethanolic stock solution into a PDMS entrance chamber, resulting in a final concentration of ~5 μM. Ion channel recordings were performed at an applied potential of +100 mV, using a patch-clamp amplifier system, as previously described.[13] Current spikes or steps with multiple conductance levels occurred within 1 h after the introduction of alamethicin (Figure 6b). Figure 6c is the corresponding histogram of the current trace shown in Figure 6b. For alamethicin in suspended lipid bilayers, channel openings usually appear in a steplike fashion in the current versus time trace.[57] However, we, recently, showed that this is not the case with respect to carbon nanotube electrodes with lipid bilayers formed by physisorption,[13] although, it does approach that of steps using graphene.[14] In ref 13, we developed a circuit model, taking into account the ultrasmall quantum capacitance of carbon nanotubes, which explained this waveform semiquantitatively. In this new work using tBLM (instead of physisorbed LB), we also observe a waveform of spikes, rather than steps, consistent with the model we developed in ref 13. Most of the current spikes or steps only lasted several milliseconds or even submilliseconds, which is consistent with our study of

the SLB-polymer-SWNT platform.[13] More interestingly, we observed more frequent openings/closings of the alamethicin channel in this work than those observed in our study of the SLB-polymer-SWNT platform. The detailed mechanism is unclear, but we speculate that after incorporation into the tBLM ion channels have to stay in close proximity to the SWNTs, as compared with the much thicker polymer layer due to the short oligo-PEG tether length, which could result in great improvement of the sensitivity of SWNTs in electrolytes because of less ionic screening.[47]

Our work has used electrical measurements (both EIS and single ion channel events) to demonstrate that both alamethicin and α-HL are electrophysiologically active in our tBLMs. This indicates that a water layer is present in the interstitial space between the tBLM and the substrate. However, without neutron scattering data, we cannot quantify the hydration level or thickness of the water layer. This remains an important topic for future studies. Just as Cornell et al.[25–27] laid the foundation for tBLM on Au, which resulted in many years of studies on the hydration level and water layer thickness between the tBLM and the substrate, [28–32] we expect a similar, comprehensive series of future papers could elucidate this relationship for tBLM on oxides. Our work demonstrates the proof of concept of this approach to several classes of nanoelectronic devices, and therefore, we believe such future studies are well justified.

4.   CONCLUSIONS

In conclusion, a new architecture of tethered lipid bilayers on oxide surfaces has been developed by step-by-step stacking of three functional molecular blocks: GOPS silane, $CA(PEG)_8$ oligo-PEG spacer, and DOPE lipid via three well-established chemical reactions. The silane-based tether chemistry was confirmed by AFM and XPS from the morphology evolution of the surface as well as the chemical components of the functional groups in each reaction stage. A uniformly fluorescent tBLM over a GOPS-CA(PEG)8-DOPE-functionalized glass surface was observed by fluorescence microscopy, after a VF process, where the hydrophilic spacer, oligo-PEG $(CA(PEG)_8)$, plays an essential role. The fluidity of tBLM was further investigated by the FRAP technique, and additional electronic characterization via EIS provides a quantitative circuit model for the membrane −nanoelectronic interface and electronic properties. Furthermore, we have demonstrated the formation of tBLMs on ITO, silicon nanoribbon surfaces, and a high-density, random SWNT network on glass surfaces. More importantly, the tBLM structure can provide a stable, biocompatible interface between SWNT networks and lipid bilayers, and thus enable the detection of single ion channel activities with high sensitivity and high temporal resolution, demonstrating the successful integration of nanoelectronics with electrophysiology. Recent experimental results and theoretical interpretations have demonstrated single charge sensing of electrolyte-gated SWNT FETs.[47,58,59] Therefore, this new tBLM-SWNT platform opens up new possibilities for the study of the transport properties of single ions through ion channel pores, potentially opening up a new area in studies of fundamental electrophysiology. In addition, this silane chemistry-based approach can be applied to various nanostructures and nanoelectronics, such as 0d semiconducting particles (quantum dots) with native or grown/deposited oxide shells,[60] metallic nanoparticles, such as iron oxide with native oxide,[61] dielectric coated 1d nanowires/

nanotubes, and 2d nanomaterials, and even for carbon nanotubes and graphene, structures, which can readily be functionalized to contain —OH side groups by design. This work provides a strategy to conveniently build up biocompatible interfaces on nanostructures and nanoelectronic devices, enabling future advances in nanotechnology and nanomaterials, to be applied to emerging problems in fundamental biology and electrophysiology.

Supplementary Material

Refer to Web version on PubMed Central for supplementary material.

ACKNOWLEDGMENTS

REFERENCES

(1). Noy A Bionanoelectronics. Adv. Mater 2011, 23, 807–820. [PubMed: 21328478]

(2). Martinez JA; Misra N; Wang Y; Stroeve P; Grigoropoulos CP; Noy A Highly Efficient Biocompatible Single Silicon Nanowire Electrodes with Functional Biological Pore Channels. Nano Lett. 2009, 9, 1121–1126. [PubMed: 19203205]

(3). Dabkowska AP; Niman CS; Piret G; Persson H; Wacklin HP; Linke H; Prinz CN; Nylander T Fluid and Highly Curved Model Membranes on Vertical Nanowire Arrays. Nano Lett. 2014, 14, 4286–4292. [PubMed: 24971634]

(4). Zhou X; Moran-Mirabal JM; Craighead HG; McEuen PL Supported Lipid Bilayer/carbon Nanotube Hybrids. Nat. Nanotechnol 2007, 2, 185–190. [PubMed: 18654251]

(5). Michel R; Gradzielski M Experimental Aspects of Colloidal Interactions in Mixed Systems of Liposome and Inorganic Nanoparticle and Their Applications. Int. J. Mol. Sci 2012, 13, 11610–11642. [PubMed: 23109874]

(6). Sackmann E Supported Membranes: Scientific and Practical Applications. Science 1996, 271, 43–48. [PubMed: 8539599]

(7). Bayley H; Cremer PS Stochastic Sensors Inspired by Biology. Nature 2001, 413, 226–230. [PubMed: 11557992]

(8). Cremer PS; Boxer SG Formation and Spreading of Lipid Bilayers on Planar Glass Supports. J. Phys. Chem. B 1999, 103, 2554–2559.

(9). Castellana ET; Cremer PS Solid Supported Lipid Bilayers: From Biophysical Studies to Sensor Design. Surf. Sci. Rep 2006, 61, 429–444.

(10). Tanaka M; Sackmann E Polymer-Supported Membranes as Models of the Cell Surface. Nature 2005, 437, 656–663. [PubMed: 16193040]

(11). Schulz P; Garcia-Celma JJ; Fendler K SSM-Based Electrophysiology. Methods 2008, 46, 97–103. [PubMed: 18675360]

(12). Spinke J; Yang J; Wolf H; Liley M; Ringsdorf H; Knoll W Polymer-Supported Bilayer on a Solid Substrate. Biophys. J 1992, 63, 1667–1671. [PubMed: 19431869]

(13). Zhou W; Wang YY; Lim T-S; Pham T; Jain D; Burke PJ Detection of Single Ion Channel Activity with Carbon Nanotubes. Sci. Rep 2015, 5, No. 9208. [PubMed: 25778101]

(14). Wang YY; Pham TD; Zand K; Li J; Burke PJ Charging the Quantum Capacitance of Graphene with a Single Biological Ion Channel. ACS Nano 2014, 8, 4228–4238. [PubMed: 24754625]
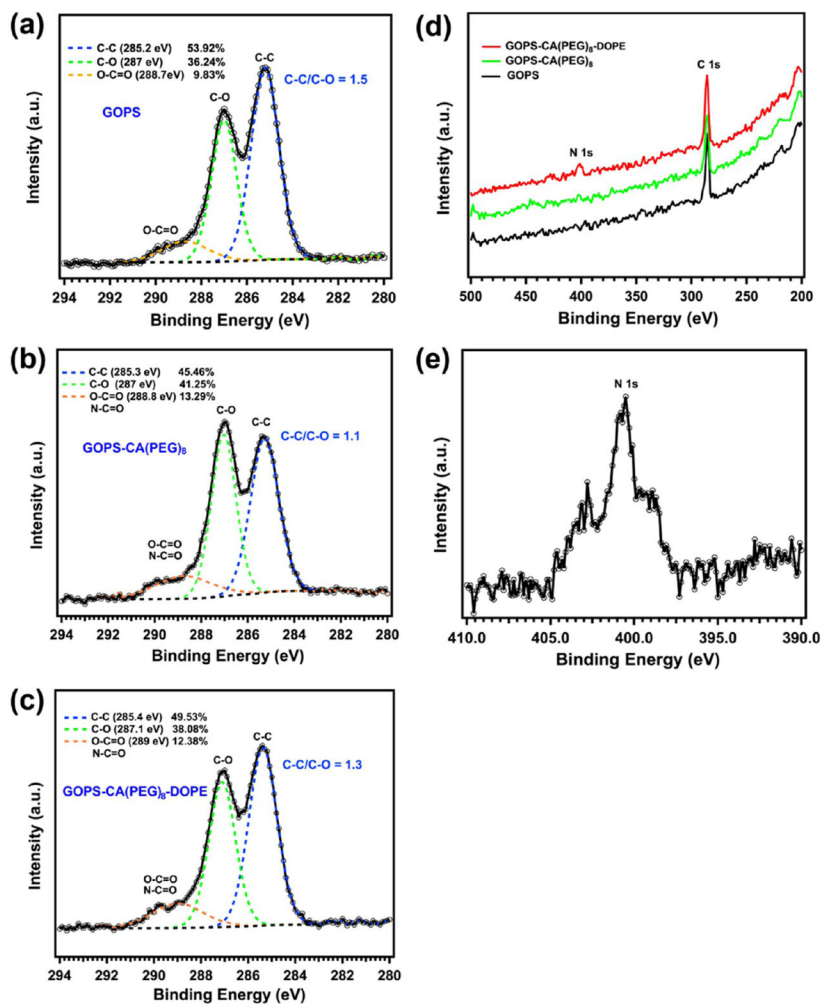
(15). Misra N; Martinez JA; Huang S-CJ; Wang Y; Stroeve P; Grigoropoulos CP; Noy A Bioelectronic Silicon Nanowire Devices Using Functional Membrane Proteins. Proc. Natl. Acad. Sci. U.S.A 2009, 106, 13780–13784. [PubMed: 19667177]

(16). VanDersarl JJ; Xu AM; Melosh NA Nanostraws for Direct Fluidic Intracellular Access. Nano Lett. 2012, 12, 3881–3886. [PubMed: 22166016]

(17). Fu T-M; Duan X; Jiang Z; Dai X; Xie P; Cheng Z; Lieber CM Sub-10-Nm Intracellular Bioelectronic Probes from Nanowire-Nanotube Heterostructures. Proc. Natl. Acad. Sci. U.S.A 2014, 111, 1259–1264. [PubMed: 24474745]

(18). Duan X; Gao R; Xie P; Cohen-Karni T; Qing Q; Choe HS; Tian B; Jiang X; Lieber CM Intracellular Recordings of Action Potentials by an Extracellular Nanoscale Field-Effect Transistor. Nat. Nanotechnol 2012, 7, 174–179.

(19). Yan R; Park J-H; Choi Y; Heo C-J; Yang S-M; Lee LP; Yang P Nanowire-Based Single-Cell Endoscopy. Nat. Nanotechnol 2012, 7, 191–196.

(20). Tian B; Cohen-Karni T; Qing Q; Duan X; Xie P; Lieber CM Three-Dimensional, Flexible Nanoscale Field-Effect Transistors as Localized Bioprobes. Science 2010, 329, 830–834. [PubMed: 20705858]

(21). Tanaka M; Sackmann E Supported Membranes as Biofunctional Interfaces and Smart Biosensor Platforms. Phys. Status Solidi A 2006, 203, 3452–3462.

(22). Goddard JM; Erickson D Bioconjugation Techniques for Microfluidic Biosensors. Anal. Bioanal. Chem 2009, 394, 469–479. [PubMed: 19280179]

(23). Vyazovkin S; Sbirrazzuoli N Mechanism and Kinetics of Epoxy–Amine Cure Studied by Differential Scanning Calorimetry. Macromolecules 1996, 29, 1867–1873.

(24). Hermanson GT Bioconjugate Techniques; Academic Press: New York, NY, 1996.

(25). Raguse B; Braach-Maksvytis V; Cornell BA; King LG; Osman PDJ; Pace RJ; Wieczorek L Tethered Lipid Bilayer Membranes: Formation and Ionic Reservoir Characterization. Langmuir 1998, 14, 648–659.

(26). Krishna G; Schulte J; Cornell BA; Pace R; Wieczorek L; Osman PD Tethered Bilayer Membranes Containing Ionic Reservoirs: The Interfacial Capacitance. Langmuir 2001, 17, 4858–4866.

(27). Krishna G; Schulte J; Cornell BA; Pace RJ; Osman PD Tethered Bilayer Membranes Containing Ionic Reservoirs: Selectivity and Conductance. Langmuir 2003, 19, 2294–2305.

(28). McGillivray DJ; Valincius G; Vanderah DJ; Febo-Ayala W; Woodward JT; Heinrich F; Kasianowicz JJ; Lösche M Molecular-Scale Structural and Functional Characterization of Sparsely Tethered Bilayer Lipid Membranes. Biointerphases 2007, 2, 21–33. [PubMed: 20408633]

(29). Heinrich F; Ng T; Vanderah DJ; Shekhar P; Mihailescu M; Nanda H; Lösche M A New Lipid Anchor for Sparsely Tethered Bilayer Lipid Membranes. Langmuir 2009, 25, 4219–4229. [PubMed: 19714901]

(30). Valincius G; Meŝkauskas T; Ivanauskas F Electrochemical Impedance Spectroscopy of Tethered Bilayer Membranes. Langmuir 2012, 28, 977–990. [PubMed: 22126190]

(31). Budvytyte R; Valincius G; Niaura G; Voiciuk V; Mickevicius M; Chapman H; Goh H-Z; Shekhar P; Heinrich F; Shenoy S; Lösche M; Vanderah DJ Structure and Properties of Tethered Bilayer Lipid Membranes with Unsaturated Anchor Molecules. Langmuir 2013, 29, 8645–8656. [PubMed: 23745652]

(32). Rakovska B; Ragaliauskas T; Mickevicius M; Jankunec M; Niaura G; Vanderah DJ; Valincius G Structure and Function of the Membrane Anchoring Self-Assembled Monolayers. Langmuir 2015, 31, 846–857. [PubMed: 25525904]

(33). Atanasov V; Knorr N; Duran RS; Ingebrandt S; Offenhäusser A; Knoll W; Köper I Membrane on a Chip: A Functional Tethered Lipid Bilayer Membrane on Silicon Oxide Surfaces. Biophys. J 2005, 89, 1780–1788. [PubMed: 16127170]

(34). Wagner ML; Tamm LK Tethered Polymer-Supported Planar Lipid Bilayers for Reconstitution of Integral Membrane Proteins: Silane-Polyethyleneglycol-Lipid as a Cushion and Covalent Linker. Biophys. J 2000, 79, 1400–1414. [PubMed: 10969002]

(35). Daniel C; Sohn KE; Mates TE; Kramer EJ; Rädler JO; Sackmann E; Nickel B; Andruzzi L Structural Characterization of an Elevated Lipid Bilayer Obtained by Stepwise Functionalization of a Self-Assembled Alkenyl Silane Film. Biointerphases 2007, 2, 109–118. [PubMed: 20408645]

(36). Sangwan VK; Ortiz RP; Alaboson JMP; Emery JD; Bedzyk MJ; Lauhon LJ; Marks TJ; Hersam MC Fundamental Performance Limits of Carbon Nanotube Thin-Film Transistors Achieved Using Hybrid Molecular Dielectrics. ACS Nano 2012, 6, 7480–7488. [PubMed: 22783918]

(37). Rajan NK; Brower K; Duan X; Reed MA Limit of Detection of Field Effect Transistor Biosensors: Effects of Surface Modification and Size Dependence. Appl. Phys. Lett 2014, 104, No. 084106.

(38). Wolf S; Tauber RN Silicon Processing for the VLSI Era, Vol. 1: Process Technology; Lattice Press: Sunset Beach, CA, 1986.

(39). Sorgenfrei S; Chiu C; Gonzalez RL; Yu Y-J; Kim P; Nuckolls C; Shepard KL Label-Free Single-Molecule Detection of DNA-Hybridization Kinetics with a Carbon Nanotube Field-Effect Transistor. Nat. Nanotechnol 2011, 6, 126–132. [PubMed: 21258331]

(40). Jang LS; Keng HK Modified Fabrication Process of Protein Chips Using a Short-Chain Self-Assembled Monolayer. Biomed. Microdevices 2008, 10, 203–211. [PubMed: 17849186]

(41). Kuno A; Uchiyama N; Koseki-Kuno S; Ebe Y; Takashima S; Yamada M; Hirabayashi J Evanescent-Field Fluorescence-Assisted Lectin Microarray: A New Strategy for Glycan Profiling. Nat. Methods 2005, 2, 851–856. [PubMed: 16278656]

(42). Liu YC; Rieben N; Iversen L; Sørensen BS; Park J; Nygård J; Martinez KL Specific and Reversible Immobilization of Histidine-Tagged Proteins on Functionalized Silicon Nanowires. Nanotechnology 2010, 21, No. 245105. [PubMed: 20498527]

(43). Demirel G;Ça layan MO; Garipcan B; Duman M; Pi kin E Oriented Immobilization of IgG on Hydroxylated Si(001) Surfaces via Protein-A by a Multiple-Step Process Based on a Self-Assembly Approach. J. Mater. Sci 2007, 42, 9402–9408.

(44). Wang M; Liechti KM; Wang Q; White JM Self-Assembled Silane Monolayers: Fabrication with Nanoscale Uniformity. Langmuir 2005, 21, 1848–1857. [PubMed: 15723481]

(45). Noy A; Miller AE; Klare JE; Weeks BL; Woods BW; DeYoreo JJ Fabrication of Luminescent Nanostructures and Polymer Nanowires by Dip-Pen Nanolithography. Nano Lett. 2002, 2, 109–112.

(46). Junghans A; Köper I Structural Analysis of Tethered Bilayer Lipid Membranes. Langmuir 2010, 26, 11035–11040. [PubMed: 20504013]

(47). Sorgenfrei S; Chiu CY; Johnston M; Nuckolls C; Shepard KL Debye Screening in Single-Molecule Carbon Nanotube Field-Effect Sensors. Nano Lett. 2011, 11, 3739–3743. [PubMed: 21806018]

(48). Nietzold C; Dietrich PM; Ivanov-Pankov S; Lippitz A; Gross T; Weigel W; Unger WES Functional Group Quantification on Epoxy Surfaces by Chemical Derivatization (CD)-XPS. Surf. Interface Anal 2014, 46, 668–672.

(49). Ariza MJ; Rodríguez-Castellon E; Rico R; Benavente J; Muñoz M; Oleinikova M X-Ray Photoelectron Spectroscopy Analysis of Di-(2-Ethylhexyl) Phosphoric Acid Activated Membranes. J. Colloid Interface Sci 2000, 226, 151–158. [PubMed: 11401359]

(50). Soumpasis DM Theoretical Analysis of Fluorescence Photobleaching Recovery Experiments. Biophys. J 1983, 41, 95–97. [PubMed: 6824758]

(51). Lin J; Szymanski J; Searson PC; Hristova K Effect of a Polymer Cushion on the Electrical Properties and Stability of Surface-Supported Lipid Bilayers. Langmuir 2010, 26, 3544–3548. [PubMed: 20175577]

(52). Casford MTL; Ge A; Kett PJN; Ye S; Davies PB The Structure of Lipid Bilayers Adsorbed on Activated Carboxy-Terminated Monolayers Investigated by Sum Frequency Generation Spectroscopy. J. Phys. Chem. B 2014, 118, 3335–3345. [PubMed: 24628457]

(53). Purrucker O; Hillebrandt H; Adlkofer K; Tanaka M Deposition of Highly Resistive Lipid Bilayer on Silicon–silicon Dioxide Electrode and Incorporation of Gramicidin Studied by Ac Impedance Spectroscopy. Electrochim. Acta 2001, 47, 791–798.

(54). Lin J; Merzlyakov M; Hristova K; Searson PC Impedance Spectroscopy of Bilayer Membranes on Single Crystal Silicon. Biointerphases 2008, 3, FA33. [PubMed: 20408667]

(55). Ruan C; Yang L; Li Y Immunobiosensor Chips for Detection of Escherichia coli O157:H7 Using Electrochemical Impedance Spectroscopy. Anal. Chem 2002, 74, 4814–4820. [PubMed: 12349988]

(56). Huang SCJ; Artyukhin AB; Misra N; Martinez JA; Stroeve PA; Grigoropoulos CP; Ju JWW; Noy A Carbon Nanotube Transistor Controlled by a Biological Ion Pump Gate. Nano Lett. 2010, 10, 1812–1816. [PubMed: 20426455]

(57). Andrew Woolley G; Wallace BA Model Ion Channels: Gramicidin and Alamethicin. J. Membr. Biol 1992, 129, 109–136. [PubMed: 1279177]

(58). Sharf T; Wang NP; Kevek JW; Brown MA; Wilson H; Heinze S; Minot ED Single Electron Charge Sensitivity of Liquid-Gated Carbon Nanotube Transistors. Nano Lett. 2014, 14, 4925–4930. [PubMed: 25160798]

(59). Bushmaker AW; Oklejas V; Walker D; Hopkins AR; Chen J; Cronin SB Single-Ion Adsorption and Switching in Carbon Nanotubes. Nat. Commun 2016, 7, No. 10475. [PubMed: 26805462]

(60). Karakoti AS; Shukla R; Shanker R; Singh S Surface Functionalization of Quantum Dots for Biotechnological Applications. Adv. Colloid Interface Sci 2015, 215, 28–45. [PubMed: 25467038]

(61). Liu Y; Li Y; Li XM; He T Kinetics of (3-Aminopropyl)-triethoxylsilane (APTES) Silanization of Superparamagnetic Iron Oxide Nanoparticles. Langmuir 2013, 29, 15275–15282. [PubMed: 24256348]

Scheme 1.
Schematic Illustration of Covalent Functionalization of a tBLM on an Oxide Surface via Step-by-Step Stacking of Three Functional Molecular Building Blocks and the VF Method

Figure 1.
High-resolution XPS C_{1s} spectra of GOPS (a), GOPS-CA(PEG)$_8$ (b) and GOPS-CA(PEG)$_8$-DOPE (c) functionalized silicon wafers, and the corresponding XPS wide scan spectra (d), and high-resolution XPS N_{1s} spectrum (e) of a GOPS-CA(PEG)$_8$-DOPE-functionalized silicon wafer.
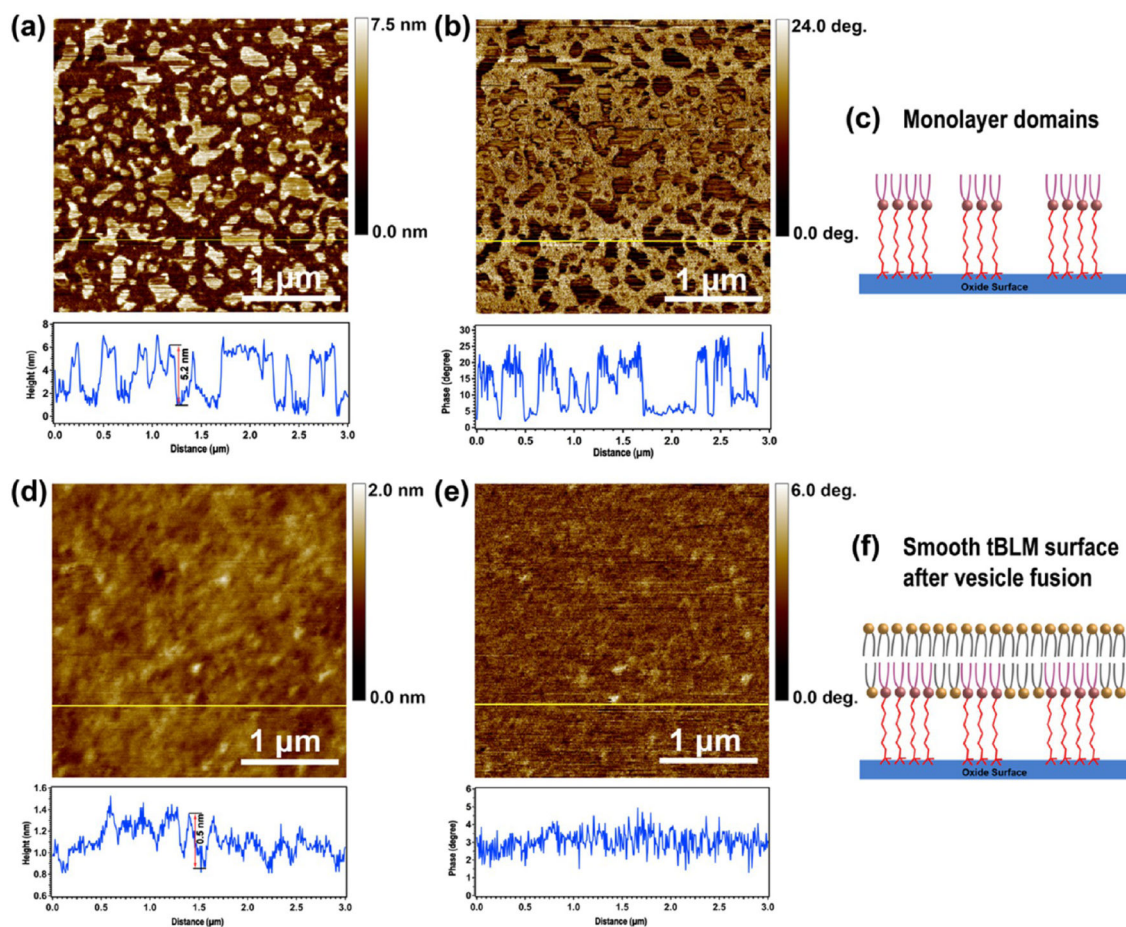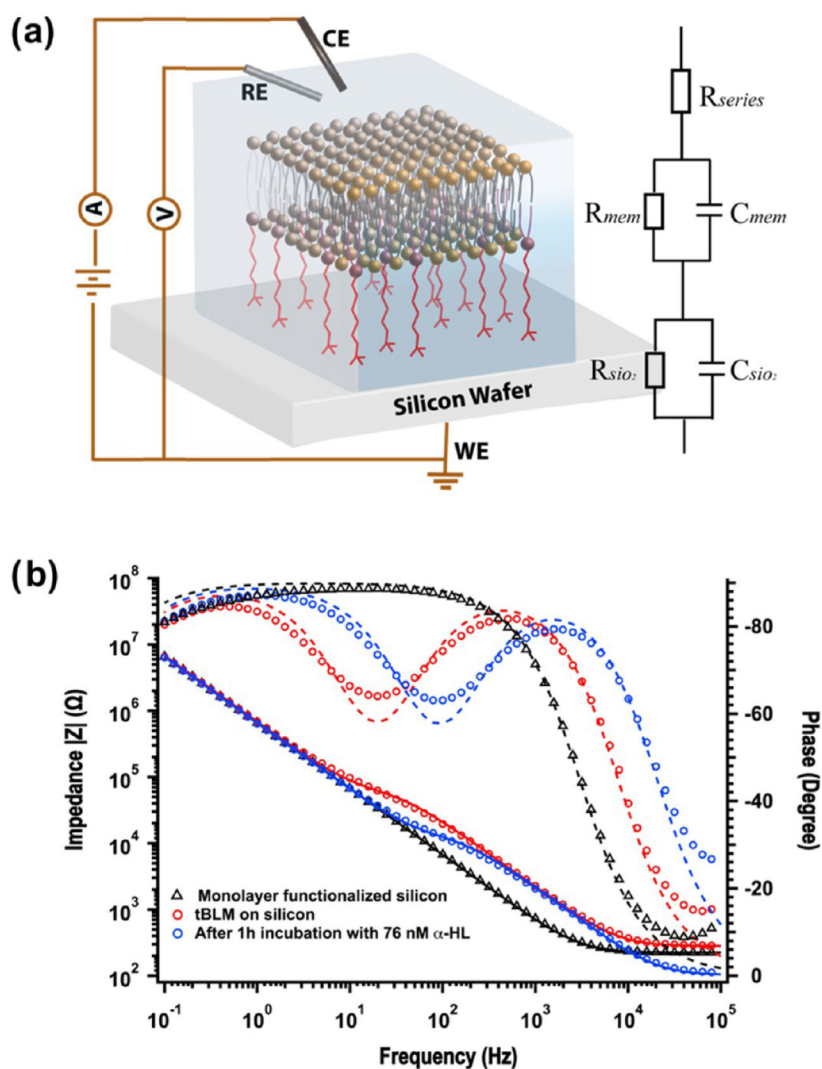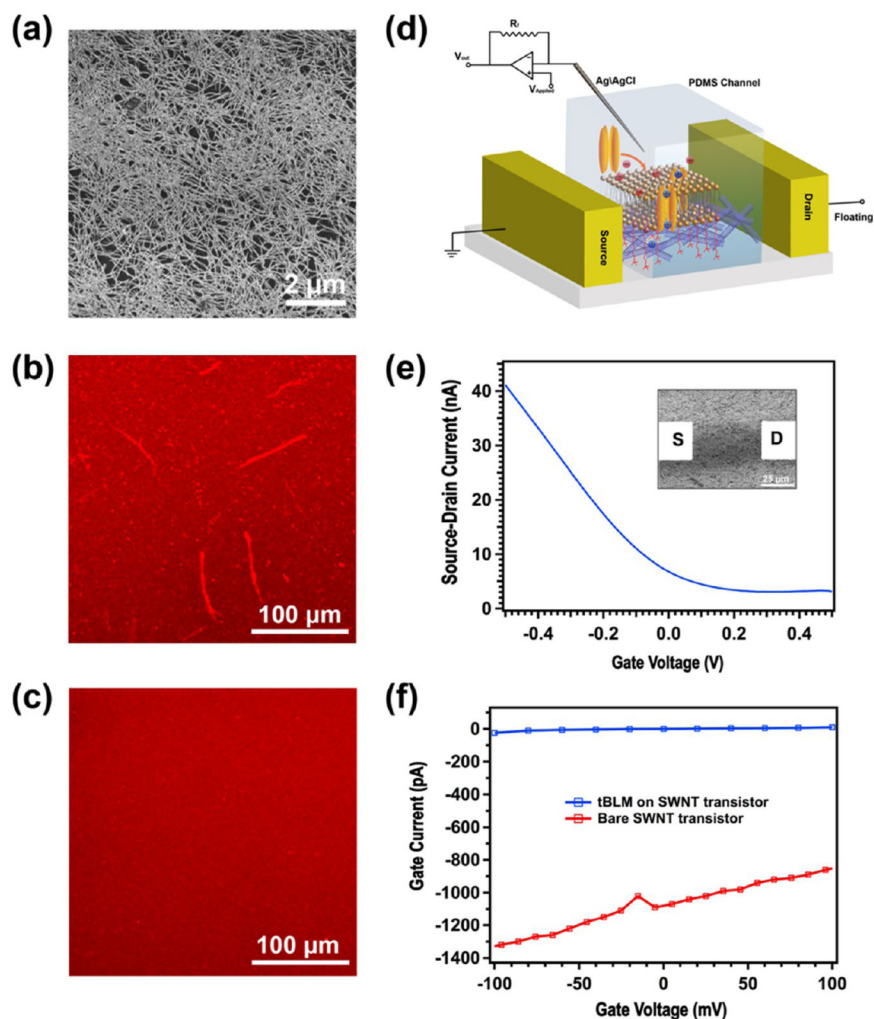
Figure 2.

AFM images of lipid monolayer-functionalized silicon wafers (a, b) and tBLMs formed on the same substrate after a VF process (d, e), and the corresponding schematic illustrations of monolayer domains (c) and the smooth surface of the final tBLM structure (f). (a, d) AFM topography images. (b, e) AFM phase images. The chart below each AFM image is the height or phase profile of the horizontal line shown in the corresponding image. AFM characterizations were performed in 1× PBS buffer. It should be noted that the hydrophobic tails in the monolayer are flexible and bundled together to minimize contact with aqueous solution. (c) A simplified cartoon for illustration purposes.
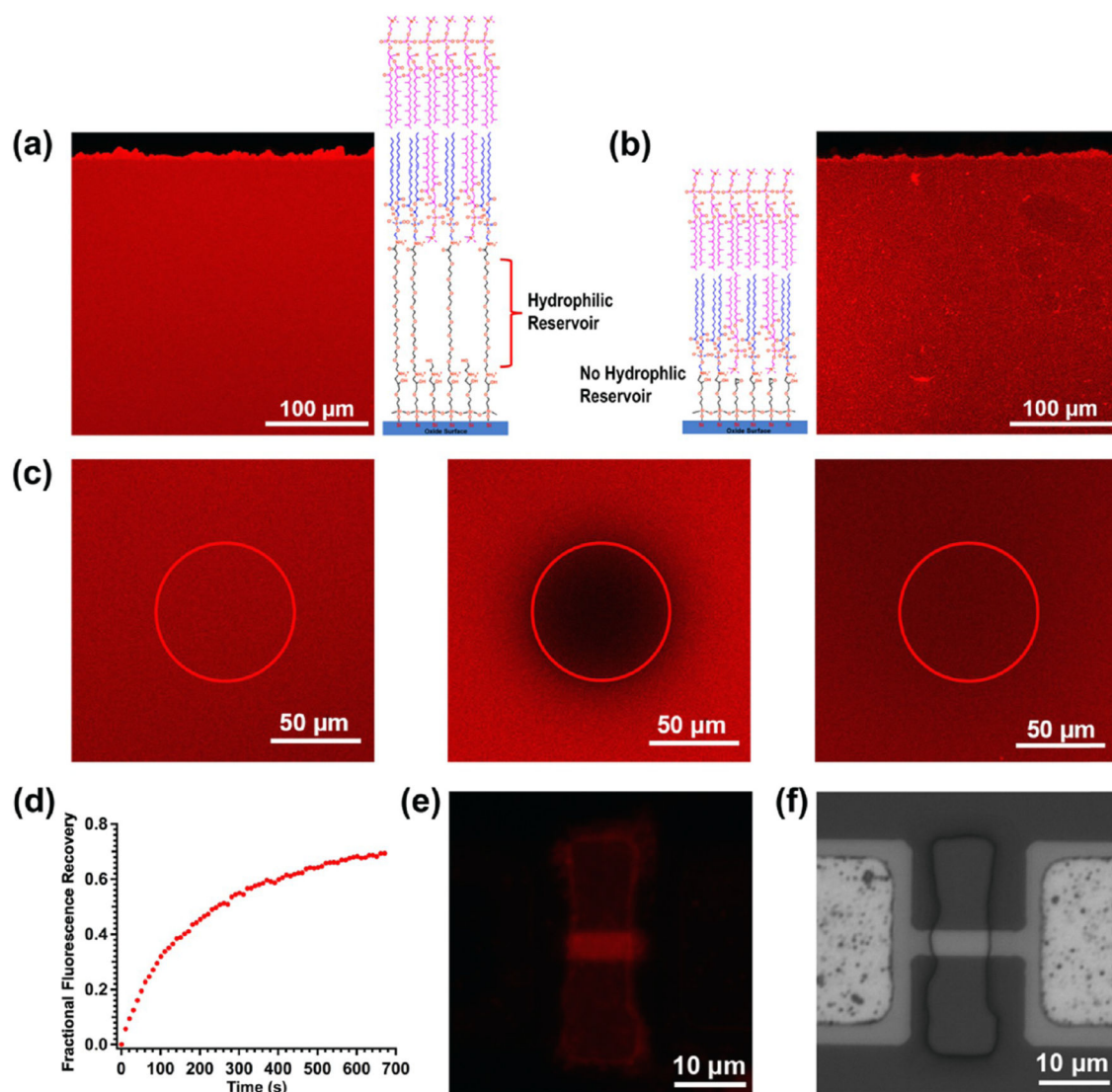
Figure 3.

Fluorescence images of the two types of tBLMs, respectively, formed on GOPS-CA(PEG)$_8$-DOPE (a) and GOPS-DOPE (b) functionalized glass slides, FRAP images (c) of the tBLM shown (a) before (left), immediately after (middle), and 670 s (right) after photobleaching, and the corresponding FRAP recovery curve (d). The fluorescence image (e) and the corresponding bright field image (f) of a silicon nanoribbon device after tBLM formation on a GOPS-CA(PEG)$_8$-DOPE-functionalized surface.
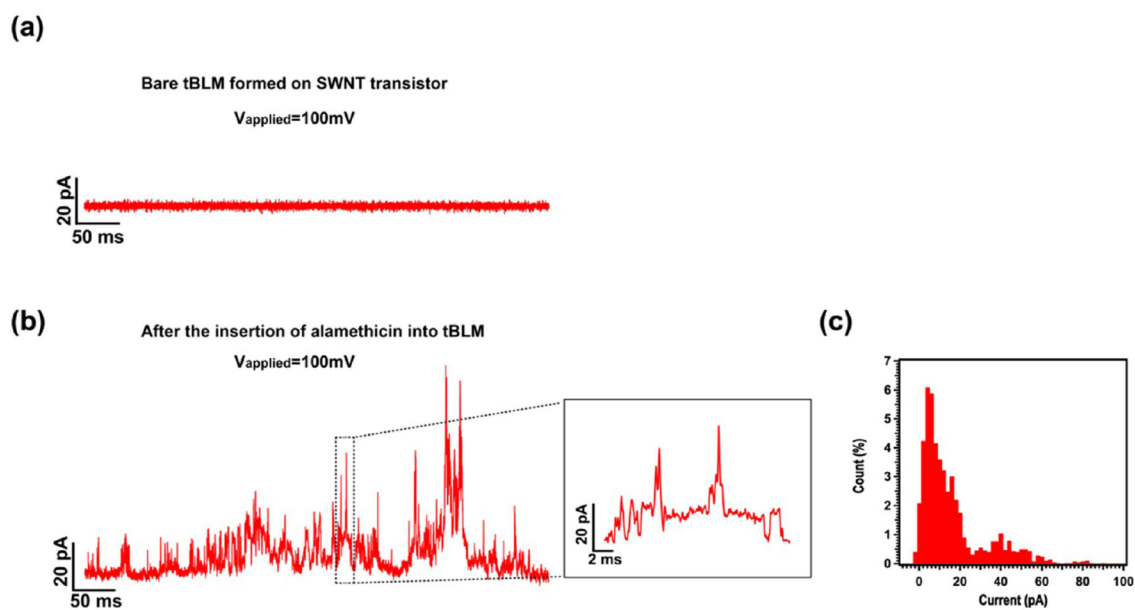
Figure 4.
(a) Schematic demonstration of the EIS experimental setup. (b) Bode plots of EIS spectra of monolayers (black triangles), and tBLMs completed with DPhPC by VF before (red circles) and after 1 h incubation with 76 nM a-HL (blue circles). The inset in (a) is the equivalent circuit model of a series resistor and two RC meshes that is used to fit the Bode plot of the tBLMs. The solid lines and dash lines in (b) represent the fitted impedance and phase curves, respectively.

Figure 5.
(a) SEM image of a high-density, random SWNT film on a glass surface. (b) Fluorescence image of the SLBs formed on the SWNT film surface. (c) Fluorescence image of the tBLM formed on the SWNT film surface. (d) Schematic demonstration of tBLM-SWNT transistor platform for ion channel recording. (e) Transfer characteristics of an electrolyte-gated SWNT field-effect transistor (FET) in $1\times$ PBS solution and at $V_{ds} = 0.1$ V. Inset: The corresponding SEM image of the SWNT FET device. (f) The gate leakage current vs gate voltage characteristics of the SWNT FET before and after tBLM functionalization.

Figure 6.
Current traces before (a) and after incorporating alamethicin (b) into a tBLM on a SWNT transistor at an applied potential of +100 mV. The inset in (b) is the enlargement of the section of the current trace enclosed by a dashed rectangle. (c) The corresponding histogram of the current trace shown in (b). All traces were recorded at a sampling frequency of 10 kHz and cutoff frequency of 5 kHz. KCl (0.5 M) in 1× PBS solution was used for the recording.

Table 1.

Resistance and Capacitance Values of Bare Silicon Wafers, Monolayer Membranes, and tBLMs Calculated from the Impedance Data Shown in Figures 3S and 4b

	R_{SiO_2} (MΩ cm^2)	C_{SiO_2} (μF cm^{-2})	R_{mem} (kΩ cm^2)	C_{mem} (μF cm^{-2})
bare silicon	1.2	2.3		
monolayer on silicon	10	2.2		
tBLM after 12 h	7.2	1.9	42.7	0.9
tBLM after 1 h incubation with α-HL	7.3	2.0	8.9	0.9